Results in Physics 7 (2017) 4287–4293

Contents lists available at ScienceDirect

Results in Physics

journal homepage: www.journals.elsevier.com/results-in-physics

Efficient amorphous silicon solar cells: characterization, optimization, and optical loss analysis

Wayesh Qarony [a,b,1], Mohammad I. Hossain [a,b,1], M. Khalid Hossain [c], M. Jalal Uddin [d], A. Haque [b], A.R. Saad [b], Yuen Hong Tsang [a,*]

[a] Dept. of Applied Physics, The Hong Kong Polytechnic University, Hung Hom, Hong Kong
[b] Dept. of Electrical & Electronic Engineering, American International University-Bangladesh (AIUB), Dhaka 1213, Bangladesh
[c] Institute of Electronics, Atomic Energy Research Establishment, Bangladesh Atomic Energy Commission, Dhaka 1349, Bangladesh
[d] Dept. of Radio Sciences and Engineering, Kwangwoon University, Seoul 01897, Republic of Korea

ARTICLE INFO

Article history:
Received 27 July 2017
Received in revised form 15 September 2017
Accepted 15 September 2017
Available online 14 November 2017

Keywords:
Superstrate p-i-n
Power loss
Quantum efficiency
Short circuit current
FDTD

ABSTRACT

Hydrogenated amorphous silicon (a-Si:H) has been effectively utilized as photoactive and doped layers for quite a while in thin-film solar applications but its energy conversion efficiency is limited due to thinner absorbing layer and light degradation issue. To overcome such confinements, it is expected to adjust better comprehension of device structure, material properties, and qualities since a little enhancement in the photocurrent significantly impacts on the conversion efficiency. Herein, some numerical simulations were performed to characterize and optimize different configuration of amorphous silicon-based thin-film solar cells. For the optical simulation, two-dimensional finite-difference time-domain (FDTD) technique was used to analyze the superstrate (p-i-n) planar amorphous silicon solar cells. Besides, the front transparent contact layer was also inquired by using SnO_2:F and ZnO:Al materials to improve the photon absorption in the photoactive layer. The cell was studied for open-circuit voltage, external quantum efficiency, and short-circuit current density, which are building blocks for solar cell conversion efficiency. The optical simulations permit investigating optical losses at the individual layers. The enhancement in both short-circuit current density and open-circuit voltage prompts accomplishing more prominent power conversion efficiency. A maximum short-circuit current density of 15.32 mA/cm^2 and an energy conversion efficiency of 11.3% were obtained for the optically optimized cell which is the best in class amorphous solar cell.

© 2017 The Authors. Published by Elsevier B.V. This is an open access article under the CC BY-NC-ND license (http://creativecommons.org/licenses/by-nc-nd/4.0/).

Introduction

A photovoltaic cell, which specifically converts sunlight into electrical energy, is one of the rising strategies to satisfy the present world's energy crisis. Crystalline silicon solar cells are exceptionally famous because of their higher conversion efficiency and piece of the pie, yet they are restricted to their massive size and higher cost [1,2]. In third generation photovoltaic innovation, silicon thin-film materials are winding-up plainly which is extremely encouraging because of their accessibility, light weight, bring down cost, and less demanding manufacture technique. In this work, to execute a efficient thin-film solar cell, hydrogenated amorphous silicon material is considered ought to their extensive variety of points of interest: higher open-circuit voltage, high absorption coefficient, adequate carrier lifetime, low manufacturing cost, and in particular it is conceivable to get a higher yield effectiveness by utilizing more thiner active layer [1–5]. Amorphous silicon can be likewise utilized as the best material for the execution of efficient multi-junction alongside the single-junction solar cells, where different single junction solar cells are in a series connection with each other to improve the open-circuit voltage of the thin-film solar cell [6,7]. The highest efficiency, so far, detailed for single junction planar thin-film hydrogenated amorphous silicon solar cell is 10.2% [8,9].

All through the exploration, the designed amorphous solar cell includes three original parts. In the optical model, intrinsic amorphous silicon is sandwiched between p-doped and n-doped materials to the excellent separation of the carriers into free charges because of the electric field at the p-n junction [10]. Also, it upgrades the volume of the space charge area to build the measure of the effective thickness, in this way encouraging more carriers to be separated into free charges. Therefore, the choice of appropriate

* Corresponding author.
E-mail address: yuen.tsang@polyu.edu.hk (Y.H. Tsang).
[1] Authors contributed equally to this work.

https://doi.org/10.1016/j.rinp.2017.09.030
2211-3797/© 2017 The Authors. Published by Elsevier B.V.
This is an open access article under the CC BY-NC-ND license (http://creativecommons.org/licenses/by-nc-nd/4.0/).

materials utilized as various layers of the solar cell assumes a unique part to examine electrical and optical execution parameters to accomplish highest conceivable efficiency. Besides, the examinations on transparent conductive oxide additionally demonstrates essential attributes, to trap and absorb adequate light inside the solar cell [4,11,12]. Moreover, a hydrogenated amorphous-based thin-film silicon solar cell was investigated utilizing various n-doped materials to observe the impact of those materials on the similar optical losses, absorption, and external quantum efficiency of the proposed solar cell structure.

Optical simulation modeling

The simulations for optical wave propagation were performed on superstrate based hydrogenated amorphous silicon solar cells on a flat glass substrate as portrayed in the cross-segmental view in Fig. 1. The optical structure of the solar cell included a 150 nm fluorine doped tin oxide (SnO_2:F) [13–17] as front transparent conductive oxide (FTCO), trailed by a 10 nm of p doped a-SiC:H layer, a 300 nm i-layer of a-Si:H, a 10 nm of n doped a-Si:H layer, and a 300 nm Ag metal back contact covered with 200 nm ZnO:Al layer back transparent conductive oxide (BTCO), was studied. In the structure, n and p doped layers were utilized as carrier transport layers, though i-layer of a-Si:H executed as photoactive layer [1,18–24]. Simulations were executed in two-dimensional (2D) case by using the finite difference time-domain (FDTD) technique [25].

Maxwell's curl equations were thoroughly followed for the electric field distribution and losses at the individual layers. The used two-dimensional FDTD calculation separated Maxwell's conditions into two distinct arrangements of conditions for transverse electric (TE) and transverse magnetic (TM) energized waves individually. The polarization of the propagated wave was considered as TE, subsequently just a single segment of the electric field, E_Z must be illuminated. With a specific end goal to gain better photo-absorption, perfect matched layer (PML) limit was assumed in Y-direction during simulation [25,26]. The simulation condition figured the electrical field distribution inside the proposed structures.

From the electric field distribution, power loss for the individual areas was computed by the Eq. (1) [25,27].

$$Q(x,y) = \frac{1}{2} c\epsilon_0 n\alpha |E(x,y)|^2. \quad (1)$$

This power-loss term leads to find the quantum efficiency, which is expressed by Eq. (2) [28,29].

$$QE = \frac{1}{P_{Opt}} \int Q(x,y)dxdy \quad (2)$$

where P_{Opt} is the incident optical power and α is the energy absorption coefficient which is related to extinction coefficient k as ($\alpha = 4\pi k/\lambda$).

After calculating external quantum efficiency and power loss within the solar cell, the short-circuit current can be computed by condition (3) [30].

$$I_{SC} = \frac{q}{hc} \int_{\lambda_{min}}^{\lambda_{max}} \lambda \cdot EQ(\lambda) \cdot S(\lambda) d\lambda \quad (3)$$

where, $S(\lambda)$ is the solar spectral irradiance for air mass 1.5.

To obtain the characteristics performance parameters under investigation, further processing of this raw data is necessary. Nevertheless, this work is a demonstration, based on only the device structure.

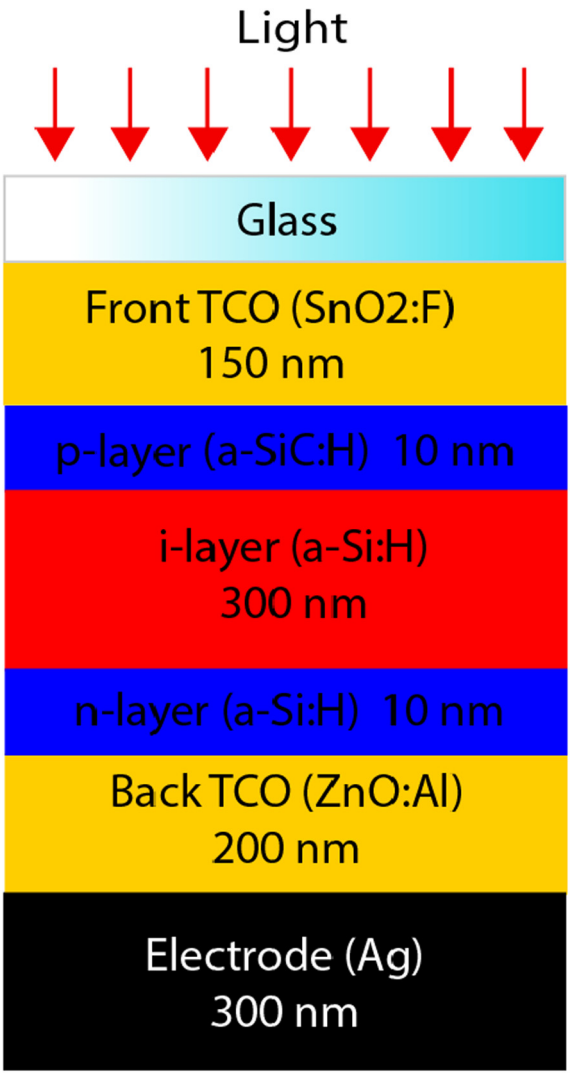

Fig. 1. Optical Structure of a-Si:H thin-film solar cell deposited on a smooth substrate.

Comparative design and loss analysis

Arrangements for the proposed optical model were changed based on doped layers and front contact materials, where each layer was subjected to the same condition for breaking down the better execution. The investigation began with the electron doped layer, changing the n-type material from a-Si:H to a-SiC:H, and inspecting the implementation of the cell. In any case, for various configurations of the optical model, thicknesses of the individual layers were kept constant, where SnO_2:F and a-SiC:H were utilized as front transparent contact and p-doped layers, respectively. To examine the total loss, reflection loss, external quantum efficiency, and parasitic absorption of a solar cell, arrangement of information were acquired over a wide range (300 nm to 800 nm) of wavelength utilizing FDTD optical simulations [25,27,31].

This work presents a valuable study on the following three optical configurations by using FDTD simulations.

Optical configuration-1: The first optical model, using SnO_2:F as front TCO, was solved selecting the same material (a-Si:H) for the i-layer and n-layer.

Optical configuration-2: In solar cell structure using SnO_2:F as front TCO, the same material (a-SiC:H) was selected for the p-layer and n-layer.

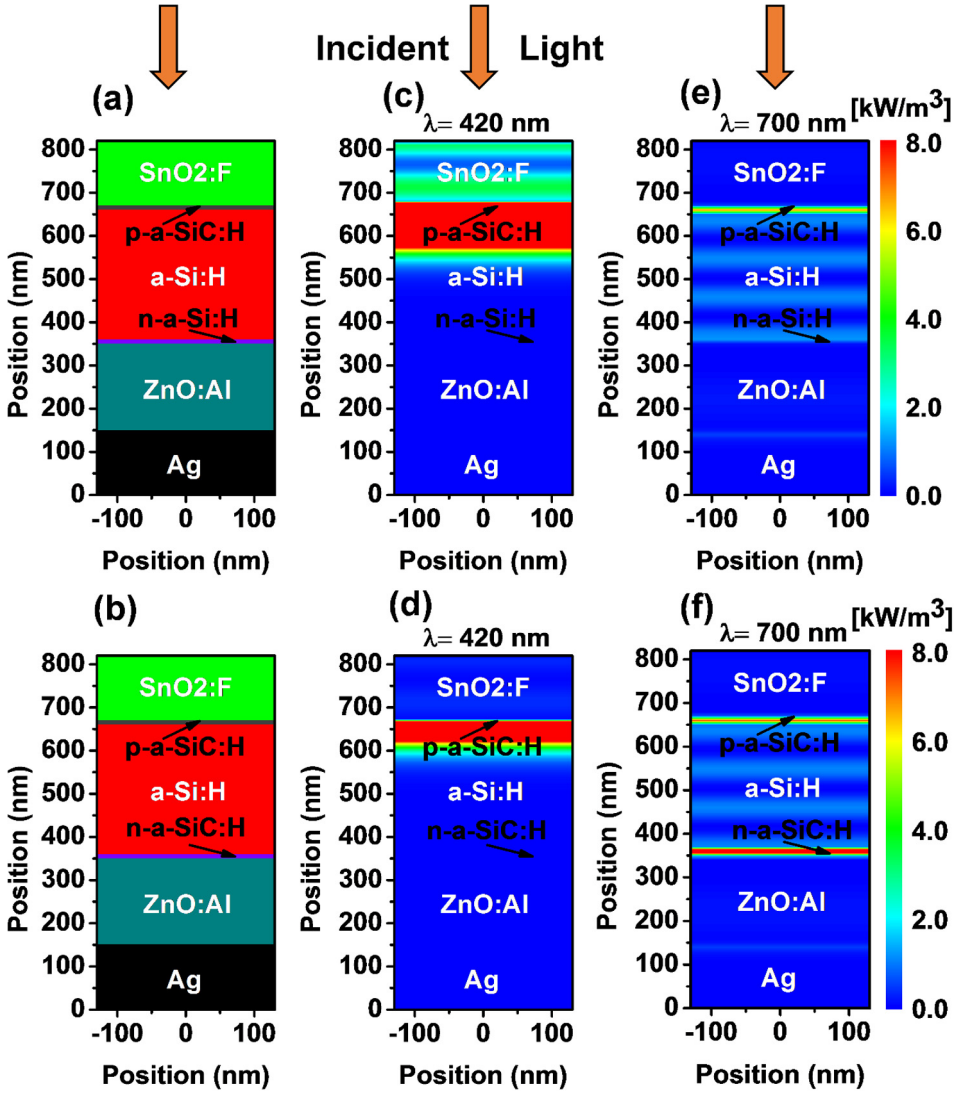

Fig. 2. Schematic cross-sectional diagram for optical configuration model-1 and 2 in (a) SnO_2:F as TCO and a-Si:H as i and n layer and (b) SnO_2:F as TCO and a-SiC:H as p and n layer, respectively with corresponding optical power losses in individual layer for monochromatic shorter and longer wavelength of (c, d) 420 nm and (e, f) 700 nm, respectively.

Optical configuration-3: The same material (a-Si:H) was selected for i-layer and n-layer; however, in this case ZnO:Al was used as front TCO.

The schematic cross-sectional diagrams of first two optical configuration models along with corresponding optical power losses in individual layers have been demonstrated in Fig. 2. The optical power loss was calculated utilizing the Eq. (1) for monochromatic shorter and longer wavelength of 420 nm and 700 nm. The amplitude of the incident photon was considered as 1000 mV/m for the optical wave propagation simulations. As the amorphous silicon material has a higher absorption coefficient in the shorter wavelength by inheritance, a relatively better photon absorption is pronounced in the shorter wavelength depicted in Fig. 2(c) and (b). The optical configuration-1 has comparatively higher power losses in the front transparent conductive oxide (SnO_2:F) than the optical configuration-2. This could be, however, because of a relatively higher amount of light reflected back from the back contact/reflector (ZnO:Al with Ag) leading to an enhanced photon absorption in the intrinsic layer as well. Due to the higher product of optical constant of a-SiC:H material in the longer wavelength, the parasitic losses in the transport layers for the optical configuration-2 is again relatively higher than the optical configuration-1. However, for the longer wavelength of 700 nm, a standing wave pattern similar to Fabry-Perot waveguide modes is observed in the active layer due to the forward and backward waves within the unit cell. At the point when the light goes starting with one layer then onto the next one, a part of the incident light is reflected back from the interface. Fig. 3(a) demonstrates a measure of light that is reflected as a component of the incident light for the wavelength range of (300 nm to 800 nm). The total reflection patterns for each model is similar up to the spectral wavelength of 650 nm, whereas it changes above this point. In the optical configuration when same material was used for i-layer and n-layer, higher reflection losses were found in the longer wavelengths which can be clarified from the power loss plots shown in Fig. 2(e). Overall, at 330 nm and 790 nm of wavelengths, minimum and maximum reflections were obtained, respectively. Fig. 3(b) outlines optical losses at the front TCO layer exhibiting almost uniform absorption over the whole optical spectral range of the models. The highest TCO loss was recorded at 300 nm, whereas the minimum is in the spectral range of 520 nm to 540 nm. Fig. 3(c) demonstrates somewhat higher loss at the p-layer in the wavelength range of 700 nm to 730 nm for the

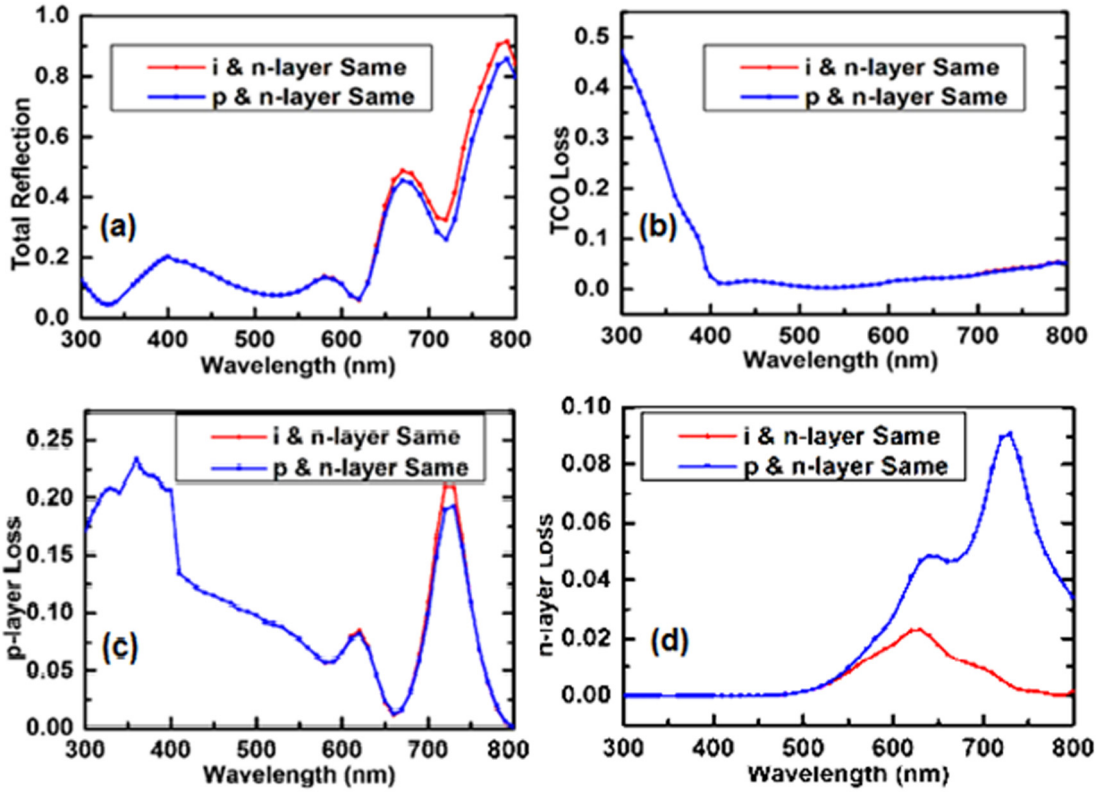

Fig. 3. Comparative (a) total reflection from the incident light, (b) loss at front transparent conductive oxide layer, (c) loss of the p-type layer, (d) loss at the n-type layer over a range of wavelengths in solar cell when doped layers were optimized.

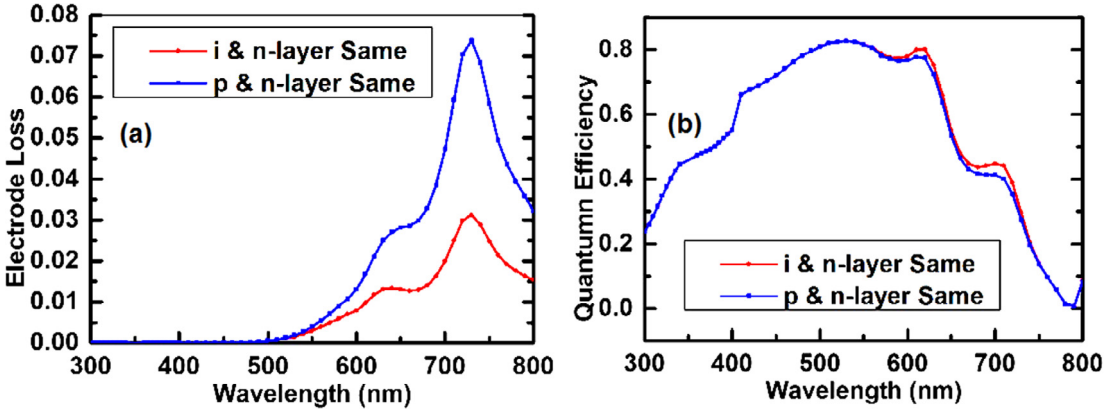

Fig. 4. Comparative (a) parasitic losses at metal reflector and (b) calculated quantum efficiencies of a solar cell over a range of wavelengths when doped layers were optimized.

i-layer and n-layer, containing a similar material. The most noteworthy loss in the p-layer was acquired at 360 nm wavelength, though the minimum was found at 660 nm. Fig. 3(d) exhibits the losses at n-layer. The figure shows that losses start expanding at the incident light wavelength of 530 nm.

The most surprising loss for a-SiC:H material, utilized as the n-type layer, was acquired at 730 nm. Despite what might be expected, for the n-type a-Si:H the most astounding loss was found at 630 nm, which compares nearly to the bandgap energy of the material. Fig. 4(a) shows the losses at the electrode, where the losses began expanding quickly with the light of wavelengths more prominent than 530 nm. Higher losses were found for the material of a-SiC:H in the optical scope of 530 nm to 800 nm. Be that as it may, the most dazing loss was recorded for the incident light wavelength of 730 nm. Also, the optics in flat amorphous silicon solar cell with the varieties of the doped layer materials were examined as far as external quantum efficiencies (EQEs) as appeared in Fig. 4(b). It can be observed from Fig. 4(b) that both QE bends demonstrate practically similar patterns except the upsetting range from 650 nm to 730 nm. This visual range compares to the most extreme photon absorption when same material was utilized for i-layer and n-layer.

It is observed that, after 800 nm, there is no absorption, which is from the inherent property of amorphous materials. A maximum of 80% absorption was found at a wavelength of 550 nm, after which the absorption was steadily diminished. On the off chance that we take a glimpse at the bends for the reflection losses, we can see that at 550 nm reflection losses were truly low. A maximum

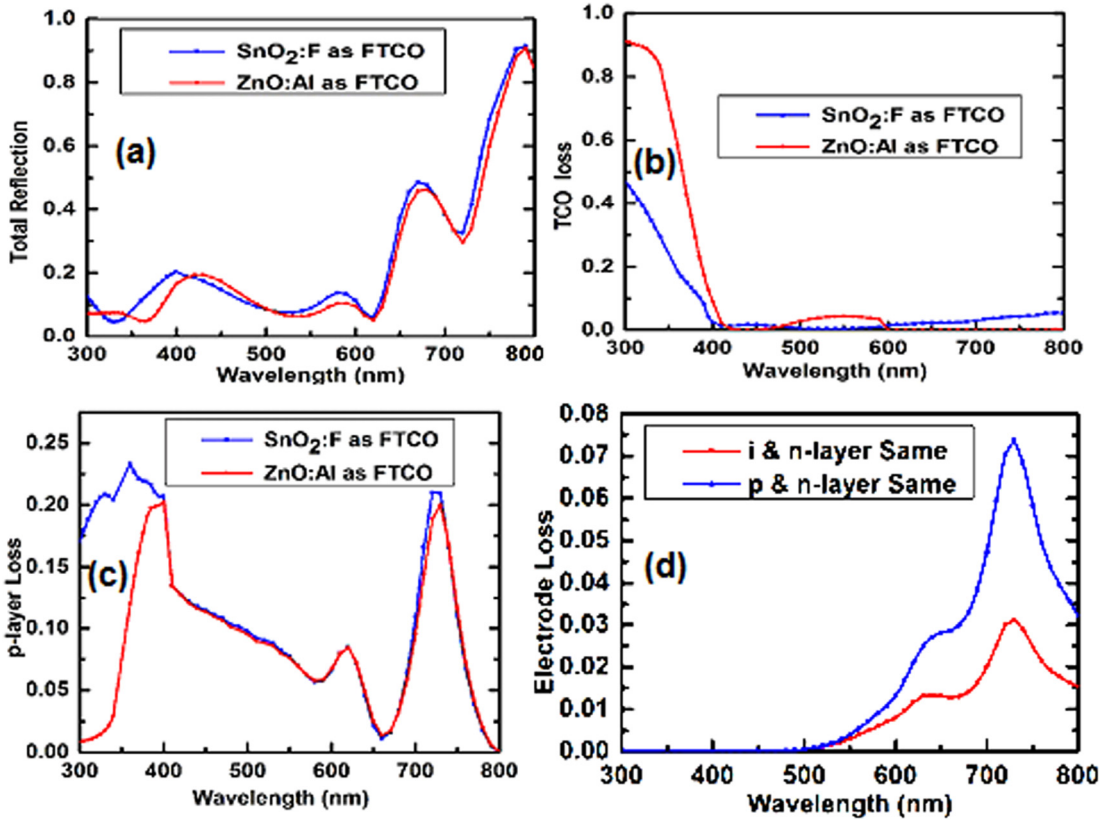

Fig. 5. Comparative (a) total reflection from the incident light, (b) loss at front transparent conductive oxide layer, (c) loss of the p-type layer, (d) loss at the p-type layer over a range of wavelengths in solar cell when TCO layer is optimized.

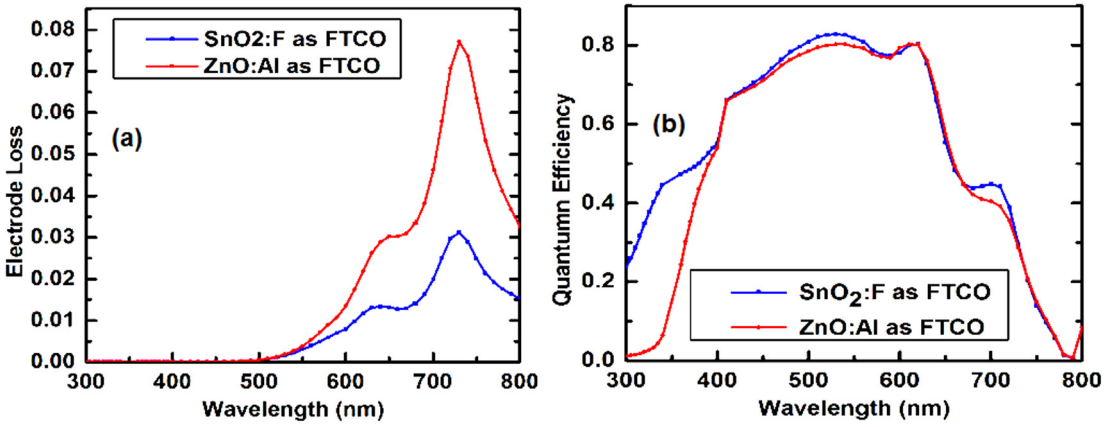

Fig. 6. Comparative (a) parasitic losses at metal reflector and (b) calculated quantum efficiencies of a solar cell over a range of wavelengths when TCO layer was optimized.

Table 1
Comparative performance parameters for three different optical models.

Optical model	J_{SC} [mA/cm^2]	V_{OC} [V]	P_{max} [mW/cm^2]	FF	η [%]
1	15.312	0.92	11.3	0.80	11.3
2	15.035	0.85	9.97	0.78	9.97
3	14.821	0.80	8.77	0.74	8.77

short-circuit current density of 15.32 mA/cm^2 was obtained when a-Si:H was utilized as n-type material. After effective investigation of the optimized optical model, the examination of the variety of front transparent contact was performed. The materials utilized for this layer were SnO_2:F and ZnO:Al. As the first study demonstrated lower losses for the n-type a-Si:H layer, henceforth, for this front TCO layer-based study, this material was further used. Fig. 5(a) demonstrates the total reflection of light, recorded from

both of the optical models. It is evident from the assumption that both of the optical models also studied all through the range of incident light utilized as a part of the simulations. The SnO_2:F front contact mirrored a somewhat bigger measure of the incident electromagnetic waves contrasted with the ZnO:Al front transparent contact. The most extreme and least estimations of total reflection were found at the light of wavelengths of 330 nm and 790 nm, respectively.

Fig. 5(b) shows the comparison between TCO losses for SnO_2:F and ZnO:Al. Lower losses were recorded when SnO2:F was utilized as FTCO material. Losses for the two materials turned out to be just about zero in the middle of 500 nm to 570 nm of wavelength. In the wavelength range of 500 nm to 800 nm, the SnO_2:F FTCO demonstrated altogether bring down losses than that of ZnO:Al front transparent contact. Fig. 5(c) shows that the losses for p-layer are higher in the range 300 nm to 400 nm and 700 nm to 730 nm. The highest loss for the p-layer was found at 360 nm wavelength for SnO_2:F. Then again, the lowest point was found at 660 nm. Fig. 5(d) shows the contact losses at the n-layer of the optical models. Fig. 6(a) demonstrates the limited losses at the anodes. Despite the fact that the optical models indicated conditional execution for the shorter wavelengths, exceptionally bring down losses were found for SnO_2:F than that of ZnO:Al inside the optical range of 530 nm to 800 nm. However, the maximum loss was recorded at 730 nm for the two models utilizing several transparent conductive oxide layers.

Fig. 6(b) exhibits the external quantum efficiencies of the two optical models used for this correlation. From the Fig. 6(b), it is seen that, SnO_2:F demonstrates higher estimations of quantum efficiencies contrasted with the ZnO:Al, over the whole range of light utilized as a part of the simulation. It likewise indicates substantially bigger locale of operation for SnO_2:F than ZnO:Al front contact. The most extreme and least quantum efficiencies are recorded for the light of 530 nm and 790 nm wavelengths, individually. The wavelengths of light between 300 nm and 400 nm, obviously demonstrated better quantum efficiency for the SnO_2:F front TCO contrasted with that of the ZnO:Al front transparent conductive oxide. Moreover, between 680 nm and 730 nm spectral range, SnO_2:F based FTCO indicates higher absorptions. From Figs. 5 and 6, it can be noted that in contrast to ZnO:Al used model, significantly better performance was found for SnO_2:F used the model in the shorter light wavelength range. The maximum loss at the n-type layer was dropped by 75.84% when the FTCO material was selected as SnO_2:F instead of ZnO:Al. At the electrode, maximum loss minimization of 59.59% was obtained for the same material of SnO_2:F rather than ZnO:Al. Thus, it could be concluded that SnO_2:F would serve as a better Front Transparent Conductive Oxide than ZnO:Al.

Comparative results and discussions

Short-circuit current densities were calculated for all the three optical model configurations using the finite-difference time-domain simulations. The estimation of the values of open circuit voltage (V_{OC}), fill factor (FF), maximum power (Pmax), and conversion efficiency (η) for each of the optical models were determined by following the conditions, which were taken from the literature [9,20].

$$V_{OC} = \frac{nkT}{q} \ln\left[\frac{j_{SC}}{j_0} + 1\right] \tag{4}$$

$$j_0 = \frac{qWN_C^{\frac{1}{2}}N_V^{\frac{1}{2}}}{\sqrt{\tau_p \tau_n}} e^{-\frac{E_g}{K_B T}} \tag{5}$$

$$FF = \frac{v_{oc} - \ln(v_{oc} - 0.72)}{v_{oc} + 1} \tag{6}$$

$$P_{max} = V_{oc} I_{SC} FF \tag{7}$$

$$\text{Efficiency}, \eta = \frac{V_{OC} I_{SC} FF}{P_{in}} \times 100\% \tag{8}$$

where n is identical to 1, open-circuit voltage is in volt [V], J_{SC} is the short-circuit current density in mA/cm^2, and J_0 the dark current density. Here P_{in} is considered for AM 1.5 case which 100 mW/cm^2. Based on simulation results and calculations, the performances of the individual optical model are summarized in Table 1.

From the Table 1, the main optical model gave higher short-current density and conversion efficiency. Along these lines, if advance examination, for example, texturing the front surface and individual layer in the cell can be performed on this optimized cell it would break the present world record efficiency of amorphous silicon based thin film solar cell.

Conclusion

The execution of the proposed single junction flat amorphous silicon solar cell has been effectively enhanced through relative examination. The simulated model of the cell traps the adequate amount of the incident light, through the introduction of the Back Transparent Conductive Oxide (BTCO) layer coated on a conventional metal electrode. We have likewise demonstrated the execution of the three several optical models, which have been built by the blends of various materials, utilized for the n-layer and the Front Transparent Conductive Oxide (FTCO) layer. The maximum conversion efficiency can be obtained for the configuration where a-Si:H and SnO_2:F is utilized as a part of the n-layer the FTCO, respectively. The maximum short-circuit current density has been obtained as 15. 32 mA/cm^2 leading to a very high conversion efficiency of 11.3%. By introducing some nanotexture or using this champion amorphous based solar cell as top cell of tandem cell, it could be possible to break the existing record efficiency in practice.

Acknowledgements

The authors want to express gratitude toward Prof. Dr. Dietmar Knipp, Dr. Rahul Dewan, and Dr. Vladislav Jovanov (Jacobs University Bremen) for educating the plan of FDTD calculation. This work is partly financially supported by The Hong Kong Polytechnic University (Grant code: G-YBFR, G-UA7N).

Conflict of interest

The author(s) declare(s) no conflict of interest regarding the publication of this paper.

References

[1] Ito H, Ogaki T, Kumakura M, Saeki S, Suzuki T, Akasaka H, et al. Changes of chemical structure of hydrogenated amorphous silicon carbide films with the application of radio-frequency bias voltages during chemical vapor deposition. Diam Relat Mater 2016;66:1–9. https://doi.org/10.1016/j.diamond.2016.03.006.

[2] Yang Z, Gao P, Zhang C, Li X, Ye J. Scattering effect of the high-index dielectric nanospheres for high performance hydrogenated amorphous silicon thin-film solar cells. Sci Rep 2016;6:30503. https://doi.org/10.1038/srep30503.

[3] Kim S, Chung J-W, Lee H, Park J, Heo Y, Lee H-M. Remarkable progress in thin-film silicon solar cells using high-efficiency triple-junction technology. Sol Energy Mater Sol Cells 2013;119:26–35. https://doi.org/10.1016/j.solmat.2013.04.016.

[4] Kim S, Lee H, Chung J-W, Ahn S-W, Lee H-M. n-Type microcrystalline silicon oxide layer and its application to high-performance back reflectors in thin-film

silicon solar cells. Curr Appl Phys 2013;13:743–7. https://doi.org/10.1016/j.cap.2012.11.017.
[5] Melskens J, van Elzakker G, Li Y, Zeman M. Analysis of hydrogenated amorphous silicon thin films and solar cells by means of Fourier Transform photocurrent spectroscopy. Thin Solid Films 2008;516:6877–81. https://doi.org/10.1016/j.tsf.2007.12.049.
[6] Kim J, Hong Z, Li G, Song T, Chey J, Lee YS, et al. 10.5% efficient polymer and amorphous silicon hybrid tandem photovoltaic cell. Nat Commun 2015;6:6391. https://doi.org/10.1038/ncomms7391.
[7] Isabella O, Smets AHM, Zeman M. Thin-film silicon-based quadruple junction solar cells approaching 20% conversion efficiency. Sol Energy Mater Sol Cells 2014;129:82–9. https://doi.org/10.1016/j.solmat.2014.03.021.
[8] Green MA, Emery K, Hishikawa Y, Warta W. Solar cell efficiency tables (version 37). Prog Photovoltaics Res Appl 2011;19:84–92. https://doi.org/10.1002/pip.1088.
[9] Matsui T, Maejima K, Bidiville A, Sai H, Koida T, Suezaki T, et al. High-efficiency thin-film silicon solar cells realized by integrating stable a-Si:H absorbers into improved device design. Jpn J Appl Phys 2015. 10.7567/JJAP.54.08KB10.
[10] Wang Y, Zhang X, Han B, Bai L, Zhao H, Yang F, et al. UV micro-imprint patterning for tunable light trapping in p-i-n thin-film silicon solar cells. Appl Surf Sci 2015;355:14–8. https://doi.org/10.1016/j.apsusc.2015.07.089.
[11] Ellmer K. Past achievements and future challenges in the development of optically transparent electrodes. Nat Photonics 2012;6:809–17. https://doi.org/10.1038/nphoton.2012.282.
[12] Zeman M, van Swaaij RACMM, Metselaar JW, Schropp REI. Optical modeling of a-Si:H solar cells with rough interfaces: effect of back contact and interface roughness. J Appl Phys 2000;88:6436–43. https://doi.org/10.1063/1.1324690.
[13] Yamaguchi S, Sugimoto Y, Fujiwara H. Characterization of textured SnO_2: F layers by ellipsometry using glass-side illumination. Thin Solid Films 2013;534:149–54. https://doi.org/10.1016/j.tsf.2013.02.018.
[14] Gao Q, Jiang H, Li C, Ma Y, Li X, Ren Z, et al. Tailoring of textured transparent conductive SnO_2:F thin films. J Alloys Compd 2013;574:427–31. https://doi.org/10.1016/j.jallcom.2013.05.108.
[15] Bhachu DS, Waugh MR, Zeissler K, Branford WR, Parkin IP. Textured fluorine-doped tin dioxide films formed by chemical vapour deposition. Chem A Eur J 2011;17:11613–21. https://doi.org/10.1002/chem.201100399.
[16] Moholkar AV, Pawar SM, Rajpure KY, Bhosale CH, Kim JH. Effect of fluorine doping on highly transparent conductive spray deposited nanocrystalline tin oxide thin films. Appl Surf Sci 2009;255:9358–64. https://doi.org/10.1016/j.apsusc.2009.07.035.
[17] Miao D, Zhao Q, Wu S, Wang Z, Zhang X, Zhao X. Effect of substrate temperature on the crystal growth orientation of SnO_2:F thin films spray-deposited on glass substrates. J Non Cryst Solids 2010;356:2557–61. https://doi.org/10.1016/j.jnoncrysol.2010.06.076.
[18] Qingwen D, Xiaoliang W, Hongling X, Zeyu M, Xiaobin Z, Qifeng H, et al. Theoretical investigation of efficiency of a p-a-SiC:H/i-a-Si:H/n-μc-Si solar cell. J Semicond 2010;31:103003. https://doi.org/10.1088/1674-4926/31/10/103003.
[19] Li SX, Cao YQ, Xu J, Rui YJ, Li W, Chen KJ. Hydrogenated amorphous silicon-carbide thin films with high photo-sensitivity prepared by layer-by-layer hydrogen annealing technique. Appl Surf Sci 2013;270:287–91. https://doi.org/10.1016/j.apsusc.2012.12.176.
[20] Lee JE, Park JH, Cho J-S, Chung J-W, Song J, Kim D, et al. Analysis on the interfacial properties of transparent conducting oxide and hydrogenated p-type amorphous silicon carbide layers in p–i–n amorphous silicon thin film solar cell structure. Thin Solid Films 2012;520:6007–11. https://doi.org/10.1016/j.tsf.2012.04.081.
[21] Pantelica D, Ionescu P, Petrascu H, Dracea MD, Statescu M, Matei E, et al. Characterization of hydrogenated and deuterated silicon carbide films codeposited by magnetron sputtering. Nucl Instrum Methods Phys Res B 2016;371:322–6. 10.1016/j.nimb.2015.10.060..
[22] Rakić AD, Djurišić AB, Elazar JM, Majewski ML. Optical properties of metallic films for vertical-cavity optoelectronic devices. Appl Opt 1998;37:5271. https://doi.org/10.1364/AO.37.005271.
[23] Heinz M, Srabionyan VV, Bugaev AL, Pryadchenko VV, Ishenko EV, Avakyan LA, et al. Formation of silver nanoparticles in silicate glass using excimer laser radiation: Structural characterization by HRTEM, XRD, EXAFS and optical absorption spectra. J Alloys Compd 2016;681:307–15. https://doi.org/10.1016/j.jallcom.2016.04.214.
[24] Hüpkes J, Rech B, Kluth O, Repmann T, Zwaygardt B, Müller J, et al. Surface textured MF-sputtered ZnO films for microcrystalline silicon-based thin-film solar cells. Sol Energy Mater Sol Cells 2006;90:3054–60. https://doi.org/10.1016/j.solmat.2006.06.027.
[25] Dewan R, Marinkovic M, Noriega R, Phadke S, Salleo A, Knipp D. Light trapping in thin-film silicon solar cells with submicron surface texture. Opt Express 2009;17:23058–65. https://doi.org/10.1364/OE.17.023058.
[26] Qarony W, Jui YA, Das GM, Mohsin T, Hossain MI, Islam SN. Optical analysis in CH3NH3PbI3 and CH3NH3PbI2Cl based thin-film perovskite solar cell. Am J Energy Res 2015;3:19–24. https://doi.org/10.12691/AJER-3-2-1.
[27] Jovanov V, Palanchoke U, Magnus P, Stiebig H, Hüpkes J, Sichanugrist P, et al. Light trapping in periodically textured amorphous silicon thin film solar cells using realistic interface morphologies. Opt Express 2013;21:A595. https://doi.org/10.1364/OE.21.00A595.
[28] Dewan R, Vasilev I, Jovanov V, Knipp D. Optical enhancement and losses of pyramid textured thin-film silicon solar cells. J Appl Phys 2011;110. https://doi.org/10.1063/1.3602092.
[29] Tamang A, Sai H, Jovanov V, Bali SIH, Matsubara K, Knipp D. On the interplay of interface morphology and microstructure of high-efficiency microcrystalline silicon solar cells. Sol Energy Mater Sol Cells 2016;151:81–8. https://doi.org/10.1016/j.solmat.2016.02.018.
[30] Palanchoke U, Jovanov V, Kurz H, Obermeyer P, Stiebig H, Knipp D. Plasmonic effects in amorphous silicon thin film solar cells with metal back contacts. Opt Express 2012;20:6340–7. https://doi.org/10.1364/OE.20.006340.
[31] Tamang A, Hongsingthong A, Jovanov V, Sichanugrist P, Khan BA, Dewan R, et al. Enhanced photon management in silicon thin film solar cells with different front and back interface texture. Sci Rep 2016;6:29639. https://doi.org/10.1038/srep29639.